Along-strike seismotectonic segmentation reflecting megathrust seismogenic behavior

Ehsan Kosari[1*], Matthias Rosenau[1], Sabrina Metzger[1], Onno Oncken[1]

[1]*Helmholtz Centre Potsdam, GFZ German Research Centre for Geosciences, Potsdam, Germany*

*ehsan.kosari@gfz-potsdam.de

matthias.rosenau@gfz-potsdam.de

sabrina.metzger@gfz-potsdam.de

onno.oncken@gfz-potsdam.de

The final version of this manuscript has been published in Geology: https://doi.org/10.1130/G51115.1

ABSTRACT

Understanding the along-strike seismogenic behavior of the megathrusts is crucial to anticipate seismic hazards in the subduction zones. However, if and how the spatiotemporal frictional heterogeneity (high and low kinematic coupling) at depth feeds back into the upper-plate deformation pattern and how the upper-plate elastic signals and permanent records may correlate has yet to be fully understood. Hence, we mimic subduction megathrust seismic cycles using an analog seismotectonic model of an elastoplastic wedge overlying a frictionally heterogeneous megathrust. Coseismically, the zone above the down-dip limit of the aseismic and seismogenic patches undergoes extension and contraction, respectively, while the strain state shows a switch in polarity from the coseismic to the interseismic. The down-dip limit of the creeping zone produces permanent along-strike extension or contraction, depending on the frictional barrier strength. Our experiments show that the frictional locking heterogeneity generates more segmented along-strike strain patterns elastically (short-term) than permanently (long-term). Moreover, our results suggest that along-strike upper-plate strain patterns could serve as a proxy for interpreting persistent lateral variations of seismogenic behavior in subduction megathrusts.

INTRODUCTION

Subduction megathrusts contain an assemblage of seismic asperities (frictionally locked) and aseismic barriers (frictionally unlocked). This frictional heterogeneity is inferred from short-term, instrumental observations of the seismic cycle deformation (e.g., Klotz et al., 2001). Along-strike frictional heterogeneity (AFH) has been inferred along a number of subduction zones by assessing co- and post-seismic slip patterns of large earthquakes (Hsu et al., 2006; Pritchard and Simons, 2006), variation of slow earthquakes activity on the interface (Baba et al., 2020), seismic tomography of megathrust (Hua et al., 2020), and spatial patterns of coupling (Métois et al., 2013; Loveless and Meade, 2016; Jolivet et al., 2020). Also, long-term records, such as abrupt relative sea-level changes recorded in coastal stratigraphy and foraminifera, trench-parallel gravity signatures, and morphotectonics records (Song and Simons, 2003; Wells et al., 2003; Saillard et al., 2017; Kemp et al., 2018) point at the heterogeneous seismogenic behavior of the megathrust. Processes such as variations in lithology (Ikari et al., 2013), pore fluid pressures (Li et al., 2018), and subducted structures (Wang and Bilek, 2011), have been proposed as mechanisms controlling this heterogeneity.

As of now, regardless of the processes driving the frictional heterogeneity, it remains unclear if and how elastic (short-term) observations and permanent (long-term) records in the upper-plate correlate and reflect the seismogenic behavior of the megathrust. Understanding the along-strike deformation with respect to seismogenic behavior is crucial because the size of the most hazardous, large earthquakes scales with the length of the ruptured segment(s).

Here, we present laboratory-scale experimental observations using a seismotectonic analog model of a generic subduction forearc. Laboratory experiments overcome the limitations of short instrumental records and incomplete geologic archives and allow us to readily examine the linkage between the AFH and along-strike seismotectonic segmentation of the upper-plate.

EXPERIMENTAL SETUP AND MODEL CONFIGURATION

Following the experimental seismotectonic model (Table S1 and Text S1) described in detail by Kosari et al. (2022a and 2022b), we generate sequences of analog megathrust earthquakes (stick-slip events) at the base of an elastoplastic granular wedge that evolves in response to the stress changes over hundreds of cycles. We analyze the surface displacements and strain pattern on short and long timescales akin to the seismotectonic evolution of natural forearcs (Fig. 1). Our subduction forearc model (Fig. 1A and 1B) is an initially flat top sand-rubber (50 vol.% quartz sand: 50 vol.% EPDM-rubber, size < 400 μm) wedge set up in a glass box on a 15° dipping, elastic basal rubber conveyor belt (the model slab). The latter is driven at a constant rate of 50 μm/sec, allowing stick-slip events to nucleate spontaneously in predefined “seismogenic” zones (asperities), which are embedded in a stably creeping matrix. The frictional properties of the materials used are measured with a ring-shear tester. To derive relevant friction parameters (μ: friction, C: cohesion, a–b: rate and state parameter), we carry out constant shear rate and velocity stepping tests under constant normal load (Fig. S1 and Text S1), resulting in stick-slip cycles simulating seismic cycles in case of velocity-weakening material ($a-b<0$). Velocity-neutral ($a-b=0$) and velocity-strengthening material ($a-b>0$) exhibit stable sliding mimicking aseismic creep along the megathrust. μ is approximately 0.6 for all of the materials used.

We mimic the along-strike heterogeneous spatiotemporal distribution of kinematic coupling (Rosenau et al., 2019; Kosari et al., 2022b) using three configurations (Fig. 1A-C). In all configurations, two “seismogenic” zones (hereafter “main slip patches”: MSPs) characterized by velocity weakening are separated by a central patch (CP) in which we vary the friction rate parameter mimicking megathrust asperities (frictionally locked) separated by an aseismic barrier (frictionally unlocked). The frictional properties of the CP vary as a velocity-strengthening (hereafter “VS configuration”), representing a high-stress creeping barrier, a velocity-neutral (VN) configuration, representing an intermediate-stress creeping zone (Gao and Wang, 2014), and a velocity-weakening (hereafter “VW configuration”) (Fig. 1C). The VW zone generates smaller slip events with a higher frequency (i.e., recurrence interval) than the MSPs, representing a conditionally-stable zone where small asperities are embedded in an aseismically creeping matrix.

A stereoscopic camera system captures micrometer-scale surface displacements associated with analog seismic cycles. Using digital image correlation, we derive surface velocities from which strain rates can be calculated.

SEISMIC CYCLE SURFACE DISPLACEMENT AND VORTICITY INDUCED BY SLIP AT DEPTHS

Here we summarize the surface displacement and the vertical axis rotation (i.e., vorticity) observed during the coseismic and interseismic stages (Fig. 2).

Coseismically, all the configurations produce the archetypical pattern in trenchward-directed surface displacement with convergence above the down-dip limit of the MSPs and divergence above the up-dip limit, reflecting localized slip normal to the trench at depth. The vorticities of opposite sense (clockwise v.s. counterclockwise) on the boundaries of the MSPs and CP causes along-strike divergence and convergence on top of and between the MSPs and CP (Figs. 2, S2, and S3). The counterclockwise and clockwise vorticities are induced by a heterogeneous slip at depth (i.e., high slip on MSPs, and no or small slip on CP). This coseismic slip heterogeneity results in complementary divergent and convergent displacement fields in the upper-plate above the down- and up-dip limits of the CP, respectively (Fig. 2).

The vortex magnitudes at the boundaries of the CP vary between the different configurations reflecting along-strike gradients in a trench-normal slip at depth. The vortex magnitudes decrease from VS to VN, to VW configuration, consistent with a relative increase in coseismic slip in the CP with respect to slip in MSPs. Particularly in the VS configuration, the creeping (central) patch tends not to slip coseismically, acting as a barrier. Consequently, the surface displacements show a high gradient from minimum trenchward displacement (Figs. S2 and S3) above the VS patch to maximum displacement above the MSPs. Lateral change in the surface displacement gradient is smaller in the VN configuration. A minimum lateral surface displacement gradient is observed in the VW configuration. In the VW configuration, the CP also acts as velocity-weakening (with a less negative “a-b”) and slips during the coseismic period; however, the slip magnitude is one order of magnitude smaller than the slip at the MSPs (Fig. S1).

Interseismically, the surface displacement pattern is complementary but reversed (landward directed) such that the vorticities undergo a polarity switch (i.e., counterclockwise vs. clockwise; Fig. 2D-F). Consequently, the zones of coseismic convergence become interseismically divergent. Again, the gradients of (back)slip at depth reflected by curvature in streamlines varies between the configurations indicating a low backslip in the creeping VS configuration (high vorticity) to a high backslip in the locked VW configuration (low vorticity). Notably, the quantities of surface deformation do not change significantly (i.e., coseismic and interseismic deformations significantly cancel out each other), indicating the dominant elastic nature of the model upper-plate seismic cycle deformation (Figs. 2 and S2). The backslip gradient at depth between the VS patch and the MSPs, hence frictional locking differences, is higher compared to the VN and VW configurations, explaining the surface pattern.

FROM SHORT-TERM TO LONG-TERM: ALONG-STRIKE STRAIN

The observed vorticities induce along-strike strain, which switches signs during the seismic cycle. Coseismically, the zone above the down-dip limit of the CP undergoes extension, while the zone above the down-dip limit of the MSPs contraction (Fig. 3A-C). The strain pattern above the up-dip limit is the opposite, showing contraction above the up-dip limit of the CP and extension above the up-dip limit of the MSPs. The along-strike strain segmentation generates oblique extensional zones bounding the contractional and connecting the extensional zones. All configurations create the same principal strain pattern. However, the VW configuration shows a lesser magnitude of strain compared to VS and VN. There is a switch in polarity in the strain pattern from the coseismic to the interseismic (Fig. 3D-F) such that the interseismic pattern is complementary but reversed.

Only a small amount (few %) of the observed seismic cycle strain in the upper-plate is preserved by means of the permanent strain (similar to nature; e.g., Jolivet et al., 2020) of the model forearc covering multiple seismic cycles (Fig. 3G-I). We observe a less segmented pattern in the permanent strain than in the elastic component. The long-term pattern of along-strike strain is most strongly expressed along the up-dip limit and shares similarities to the coseismic stage. The along-strike extensional strain pattern above the MSPs is quantitatively similar in all configurations. Main differences between the models are found in the low permanent strain areas on top of the downdip limit of the barrier. Accordingly, the VS and VN configurations show contraction, whereas, in the VW zone, the strain above the down-dip limit exhibits extension.

EXAMPLES FROM NATURAL SUBDUCTION MEGATHRUSTS

Our results imply that, besides other processes not represented in our model (e.g., the role of fluids), the along-strike strain pattern, controlled by the spatiotemporal variation in the kinematic coupling of the megathrusts (Fig. 4), can also be tracked as variations in upper-plate tectonic structures as well as crustal stress state along the natural subduction megathrusts.

In the Peru-Chilean subduction system, the peninsulas may act as the frequent (not persistent) barrier such that earthquake rupture may stop beneath the peninsulas. There is evidence that earthquake rupture stops beneath the Ilo Peninsula frequently (Fig. 4C) where an orthogonal normal fault system (i.e., Chololo fault system) in the Coastal Cordillera suggests an along-strike extension (Fig. 4C) (Audin et al., 2008; Loveless et al., 2010; Philibosian and Meltzner, 2020). Our experiments propose a similar pattern where a VW segment (with unfavorable frictional conditions for megathrust events) is bounded by MSPs (Fig. 4), generating trench-normal extension at the down-dip of the frequent (not persistent) barrier. The Mejillones, the Topocalma, the Arauco peninsulas as well as EW-striking reverse fault scarps in the Coastal Cordillera (Fig. 4C), formed by trench-parallel shortening, may bound the earthquake rupture extends (Allmendinger et al., 2005; Melnick et al., 2009; Victor et al., 2011; Jara-Muñoz et al., 2015; González et al., 2015). Our experiments reproduce this along-strike shortening, where two MSPs bound a VS or VN patch along the trench (Fig 3 and 4). The oblique normal faults in the Coastal Cordillera of south Chile correlate with the segmentation of the large earthquakes (i.e., 2015 Illapel, 2010 Maule, 1985 Valparaiso, 1971, 1943, and 1928 earthquakes) and their rupture extents (Barrientos, 1988; Jara-Muñoz et al., 2022). These faults in southern Chile are usually considered to be inherited crustal structures. Our experiments suggest that the coseismic stress field induces normal slip on these faults. In addition, our results propose that the oblique faults might also mark the boundary of asperity/barrier on the interface at depth (Figs. 3 and 4A-B).

The AFH may feed back into the upper-plate stress state, its orientation, and consequently, the strain pattern. A megathrust frictional transition, inferred from along-strike variations of both coupling degree and shallow slow-slip events on the megathrust, has also been proposed for the shallow portion of the Hikurangi subduction (New Zealand; Wallace, 2020, and references therein). This frictional transition appears to drive the along-strike variations of shallow tectonic stress orientations in the upper-plate derived from earthquake focal mechanisms and borehole data (Behboudi et al., 2022, and references therein). The along-strike change in megathrust seismogenic behavior has also been recorded in the Alaska convergent margin. The geodetic observations (Drooff and Freymueller, 2021) and lack of evidence for great earthquakes in marine terraces and shore platforms (Witter et al., 2014) suggest weakly coupled megathrust in the Shumagin Gap. The along-strike abrupt changes in the coupling of the megathrust might also be reflected in the upper-plate structures such that the structures in the low coupling zone may differ compared with adjacent segments (Bécel et al., 2017).

CONCLUSION

Our results suggest that the spatiotemporal pattern of the frictional locking (kinematic coupling) at depth feeds back into the along-strike upper-plate seismotectonic segmentation and has a significant control on the strain pattern and state. The zone above the down-dip limit of the aseismic and seismogenic patches undergoes extension and contraction coseismically and switches its polarity interseismically. The experiments demonstrate that the strain pattern in the upper-plate is more segmented elastically than permanently. Moreover, depending on the strength of the barriers (frictionally unlocked), the down-dip limit of the creeping zone may correlate with upper-plate along-strike extension (conditionally stable creeping zone) or contraction (intermediate to high-stress creeping zone) permanently. Furthermore, the AFH can produce oblique extension/contractional zones bounding asperities and barriers. Our observations imply that along-strike strain patterns could serve as a proxy for interpreting persistent lateral variations of seismogenic behavior in megathrusts.

ACKNOWLEDGMENTS

The authors thank Frank Neumann for his assistance during our laboratory experiments. The authors also thank GFZ Data Services for publishing the data. The uniform colormaps are adapted from Crameri, (2018).

REFERENCES CITED

Allmendinger, R.W., González, G., Yu, J., Hoke, G., and Isacks, B., 2005, Trench-parallel shortening in the Northern Chilean Forearc: Tectonic and climatic implications: GSA Bulletin, v. 117, p. 89–104, doi:10.1130/B25505.1.

Audin, L., Lacan, P., Tavera, H., and Bondoux, F., 2008, Upper plate deformation and seismic barrier in front of Nazca subduction zone: The Chololo Fault System and active tectonics along the Coastal Cordillera, southern Peru: Tectonophysics, v. 459, p. 174–185, doi:10.1016/J.TECTO.2007.11.070.

Baba, S., Takemura, S., Obara, K., and Noda, A., 2020, Slow Earthquakes Illuminating Interplate Coupling Heterogeneities in Subduction Zones: Geophysical Research Letters, v. 47, p. e2020GL088089, doi:10.1029/2020GL088089.

Barrientos, S.E., 1988, Slip distribution of the 1985 Central Chile earthquake: Tectonophysics, v. 145, p. 225–241, doi:10.1016/0040-1951(88)90197-7.

Bécel, A. et al., 2017, Tsunamigenic structures in a creeping section of the Alaska subduction zone: Nature Geoscience 2017 10:8, v. 10, p. 609–613, doi:10.1038/ngeo2990.

Behboudi, E., McNamara, D.D., Lokmer, I., Wallace, L.M., and Saffer, D.M., 2022, Spatial Variation of Shallow Stress Orientation Along the Hikurangi Subduction Margin: Insights From In-Situ Borehole Image Logging: Journal of Geophysical Research: Solid Earth, v. 127, p. e2021JB023641, doi:10.1029/2021JB023641.

Drooff, C., and Freymueller, J.T., 2021, New Constraints on Slip Deficit on the Aleutian Megathrust and Inflation at Mt. Veniaminof, Alaska From Repeat GPS Measurements: Geophysical Research Letters, v. 48, p. e2020GL091787, doi:10.1029/2020GL091787.

Gao, X., and Wang, K., 2014, Strength of stick-slip and creeping subduction megathrusts from heat flow observations: Science, v. 345, p. 1038–1041, doi:10.1126/science.1255487.

González, G., Salazar, P., Loveless, J.P., Allmendinger, R.W., Aron, F., and Shrivastava, M., 2015, Upper plate reverse fault reactivation and the unclamping of the megathrust during the 2014 northern Chile earthquake sequence: Geology, v. 43, p. 671–674, doi:10.1130/G36703.1.

Hsu, Y.J., Simons, M., Avouac, J.P., Galeteka, J., Sieh, K., Chlieh, M., Natawidjaja, D., Prawirodirdjo, L., and Bock, Y., 2006, Frictional afterslip following the 2005 Nias-Simeulue earthquake, Sumatra: Science, v. 312, p. 1921–1926, doi:10.1126/science.1126960.

Hua, Y., Zhao, D., Toyokuni, G., and Xu, Y., 2020, Tomography of the source zone of the great 2011 Tohoku earthquake: Nature Communications 2020 11:1, v. 11, p. 1–7, doi:10.1038/s41467-020-14745-8.

Ikari, M.J., Hüpers, A., and Kopf, A.J., 2013, Shear strength of sediments approaching subduction in the Nankai Trough, Japan as constraints on forearc mechanics: Geochemistry, Geophysics, Geosystems, v. 14, p. 2716–2730, doi:10.1002/GGGE.20156.

Jara-Muñoz, J., Melnick, D., Brill, D., and Strecker, M.R., 2015, Segmentation of the 2010 Maule Chile earthquake rupture from a joint analysis of uplifted marine terraces and seismic-cycle deformation patterns: Quaternary Science Reviews, v. 113, p. 171–192, doi:10.1016/J.QUASCIREV.2015.01.005.

Jara-Muñoz, J., Melnick, D., Li, S., Socquet, A., Cortés-Aranda, J., Brill, D., and Strecker, M.R., 2022, The cryptic seismic potential of the Pichilemu blind fault in Chile revealed by off-fault geomorphology: Nature Communications 2022 13:1, v. 13, p. 1–13, doi:10.1038/s41467-022-30754-1.

Jolivet, R., Simons, M., Duputel, Z., Olive, J.-A., Bhat, H.S., and Bletery, Q., 2020, IJolivet, R., Simons, M., Duputel, Z., Olive, J.-A., Bhat, H. S., & Bletery, Q. (2020). Interseismic Loading of Subduction Megathrust Drives Long-Term Uplift in Northern Chile. Geophysical Research Letters, 47(8), e2019GL085377. https://doi.org/10.1029/20: Geophysical Research Letters, v. 47, p. e2019GL085377, doi:10.1029/2019GL085377.

Kemp, A.C., Cahill, N., Engelhart, S.E., Hawkes, A.D., and Wang, K., 2018, Revising Estimates of Spatially Variable Subsidence during the A.D. 1700 Cascadia Earthquake Using a Bayesian Foraminiferal Transfer Function: Bulletin of the Seismological Society of America, v. 108, p. 654–673, doi:10.1785/0120170269.

Klotz, J., Khazaradze, G., Angermann, D., Reigber, C., Perdomo, R., and Cifuentes, O., 2001, Earthquake cycle dominates contemporary crustal deformation in Central and Southern Andes: Earth and Planetary Science Letters, v. 193, p. 437–446, doi:10.1016/S0012-821X(01)00532-5.

Kosari, E., Rosenau, M., and Oncken, O., 2022a, Strain Signals Governed by Frictional-Elastoplastic Interaction of the Upper Plate and Shallow Subduction Megathrust Interface Over Seismic Cycles: Tectonics, v. 41, p. e2021TC007099, doi:10.1029/2021TC007099.

Kosari, E., Rosenau, M., Ziegenhagen, T., and Oncken, O., 2022b, Upper Plate Response to a Sequential Elastic Rebound and Slab Acceleration During Laboratory-Scale Subduction Megathrust Earthquakes: Journal of Geophysical Research: Solid Earth, v. 127, p. e2022JB024143, doi:10.1029/2022JB024143.

Li, J., Shillington, D.J., Saffer, D.M., Bécel, A., Nedimović, M.R., Kuehn, H., Webb, S.C., Keranen, K.M., and Abers, G.A., 2018, Connections between subducted sediment, pore-fluid pressure, and earthquake behavior along the Alaska megathrust: Geology, v. 46, p. 299–302, doi:10.1130/G39557.1.

Loveless, J.P., and Meade, B.J., 2016, Two decades of spatiotemporal variations in subduction zone coupling offshore Japan: Earth and Planetary Science Letters, v. 436, p. 19–30, doi:10.1016/J.EPSL.2015.12.033.

Loveless, J.P., Pritchard, M.E., and Kukowski, N., 2010, Testing mechanisms of subduction zone segmentation and seismogenesis with slip distributions from recent Andean earthquakes: Tectonophysics, v. 495, p. 15–33, doi:10.1016/J.TECTO.2009.05.008.

Melnick, D., Bookhagen, B., Strecker, M.R., and Echtler, H.P., 2009, Segmentation of megathrust rupture zones from fore-arc deformation patterns over hundreds to millions of years, Arauco peninsula, Chile: Journal of Geophysical Research: Solid Earth, v. 114, p. 1407, doi:10.1029/2008JB005788.

Métois, M., Socquet, A., Vigny, C., Carrizo, D., Peyrat, S., Delorme, A., Maureira, E., Valderas-Bermejo, M.-C., and Ortega, I., 2013, Revisiting the North Chile seismic gap segmentation using GPS-derived interseismic coupling: Geophysical Journal International, v. 194, p. 1283–1294, doi:10.1093/GJI/GGT183.

Philibosian, B., and Meltzner, A.J., 2020, Segmentation and supercycles: A catalog of earthquake rupture patterns from the Sumatran Sunda Megathrust and other well-studied faults worldwide: Quaternary Science Reviews, v. 241, p. 106390, doi:10.1016/J.QUASCIREV.2020.106390.

Pritchard, M.E., and Simons, M., 2006, An aseismic slip pulse in northern Chile and along-strike variations in seismogenic behavior: Journal of Geophysical Research: Solid Earth, v. 111, doi:10.1029/2006JB004258.

Rosenau, M., Horenko, I., Corbi, F., Rudolf, M., Kornhuber, R., and Oncken, O., 2019, Synchronization of Great Subduction Megathrust Earthquakes: Insights From Scale Model Analysis: Journal of Geophysical Research: Solid Earth, v. 124, p. 3646–3661, doi:10.1029/2018JB016597.

Saillard, M., Audin, L., Rousset, B., Avouac, J.-P., Chlieh, M., Hall, S.R., Husson, L., and Farber, D.L., 2017, From the seismic cycle to long-term deformation: linking seismic coupling and Quaternary coastal geomorphology along the Andean megathrust: Tectonics, v. 36, p. 241–256, doi:10.1002/2016TC004156.

Song, T.R.A., and Simons, M., 2003, Large trench-parallel gravity variations predict seismogenic behavior in subduction zones: Science, v. 301, p. 630–633, doi:10.1126/science.1085557.

Victor, P., Sobiesiak, M., Glodny, J., Nielsen, S.N., and Oncken, O., 2011, Long-term persistence of subduction earthquake segment boundaries: Evidence from Mejillones Peninsula, northern Chile: Journal of Geophysical Research: Solid Earth, v. 116, doi:10.1029/2010JB007771.

Vigny, C., and Klein, E., 2022, The 1877 megathrust earthquake of North Chile two times smaller than thought? A review of ancient articles: Journal of South American Earth Sciences, v. 117, p. 103878, doi:10.1016/J.JSAMES.2022.103878.

Wallace, L.M., 2020, Slow Slip Events in New Zealand: https://doi.org/10.1146/annurev-earth-071719-055104, v. 48, p. 175–203, doi:10.1146/ANNUREV-EARTH-071719-055104.

Wang, K., and Bilek, S.L., 2011, Do subducting seamounts generate or stop large earthquakes? Geology, v. 39, p. 819–822, doi:10.1130/G31856.1.

Wells, R.E., Blakely, R.J., Sugiyama, Y., Scholl, D.W., and Dinterman, P.A., 2003, Basin-centered asperities in great subduction zone earthquakes: A link between slip, subsidence, and subduction erosion? Journal of Geophysical Research: Solid Earth, v. 108, p. 2507, doi:10.1029/2002jb002072.

Witter, R.C., Briggs, R.W., Engelhart, S.E., Gelfenbaum, G., Koehler, R.D., and Barnhart, W.D., 2014, Little late Holocene strain accumulation and release on the Aleutian megathrust below the Shumagin Islands, Alaska: Geophysical Research Letters, v. 41, p. 2359–2367, doi:10.1002/2014GL059393.

FIGURES

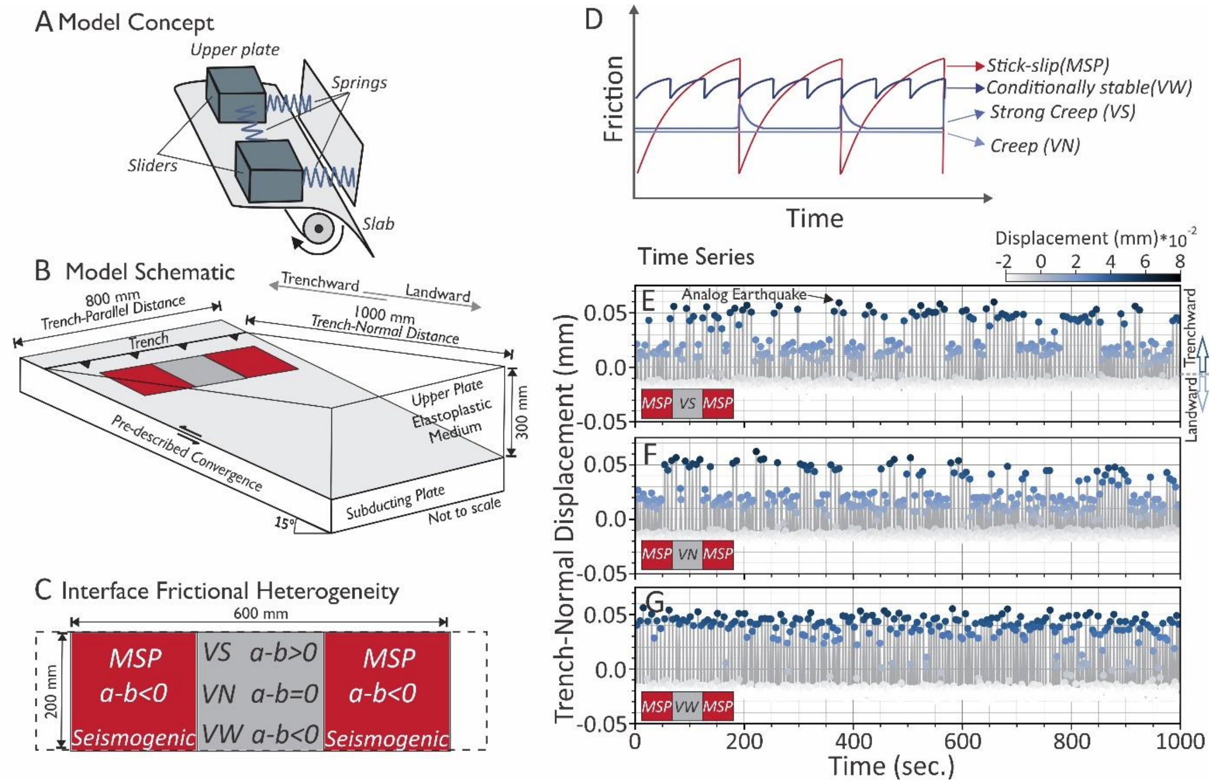

Figure 1: Model concept, geometry, configuration, and behavior: (A) coupled spring sliders (B) geometry and seismotectonic scale. The main slip patches (MSP) are separated by aseismic asperity (gray) with varying properties. The light gray interface is velocity-neutral material. (C) frictional interface heterogeneity. VS, VN, and VW represent velocity-strengthening, Velocity-neutral, and velocity-weakening material, respectively. (D) scheme of the frictional behavior of the interface over time; modified after (Gao and Wang, 2014). (E-G) surface displacement over time for the central patch being E) velocity-strengthening, F) neutral, and G) weakening.

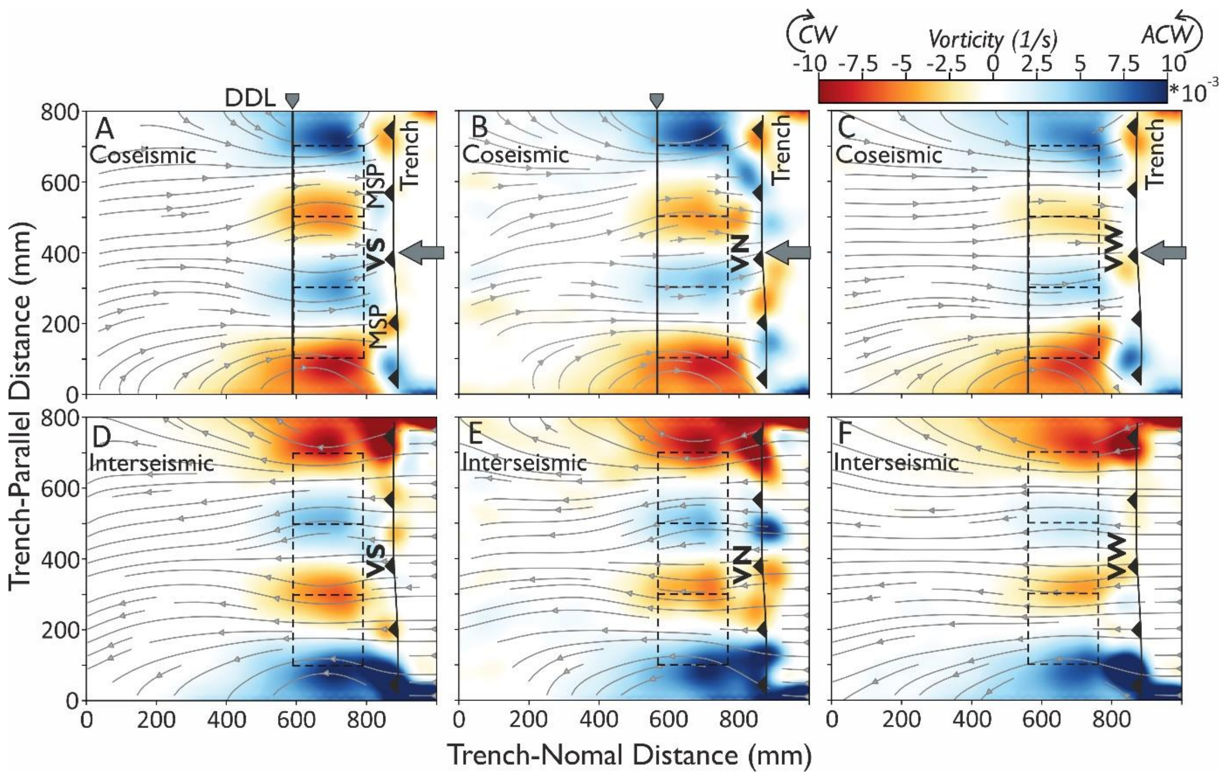

Figure 2: 2D view of surface displacement streamlines (gray lines) and colored vorticity in map view for coseismic (A-C) and interseismic (D-F) phases and different configurations (VS, VN, and VW). Dashed rectangles mark the MSPs and CP. DLL indicates the projection of the down-dip limit on the model surface. The red (warm) and blue (cold) background maps show the clockwise (CW) and counterclockwise (ACW) vorticity on the upper-plate, respectively. The large gray arrow indicates the subduction convergence.

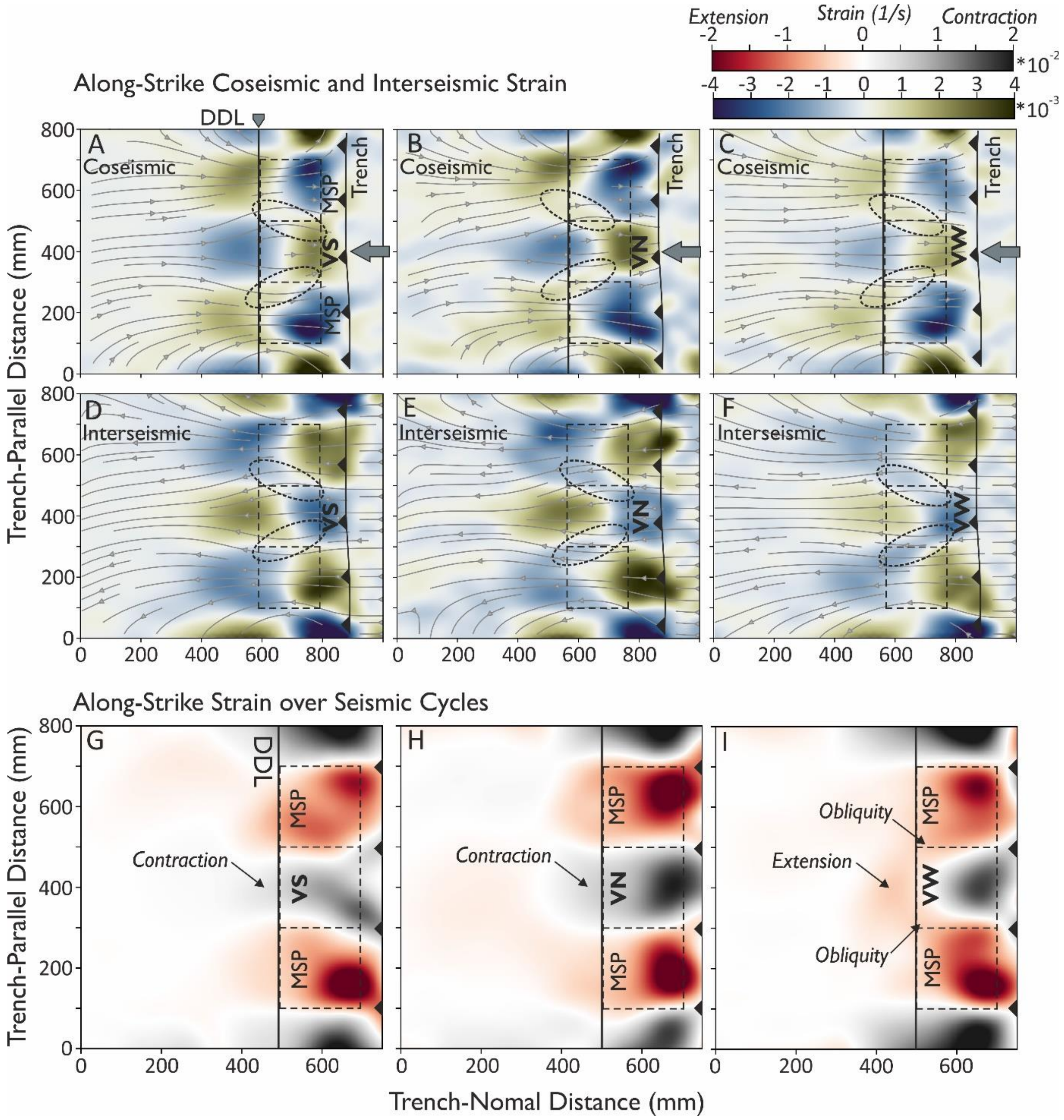

Figure 3: (A-F) Surface displacement streamlines (gray lines) overlaid on colored along-strike strain maps stacked from 10 coseismic (A-C) and interseismic (D-F) strain maps. The dashed ellipses indicate the oblique extensional/contractional zones. (G-I) Permanent upper-plate strain in VS (A), VN (B), and VW (C) configurations over 100s of seismic cycles. For all other features we refer to Figure 2.

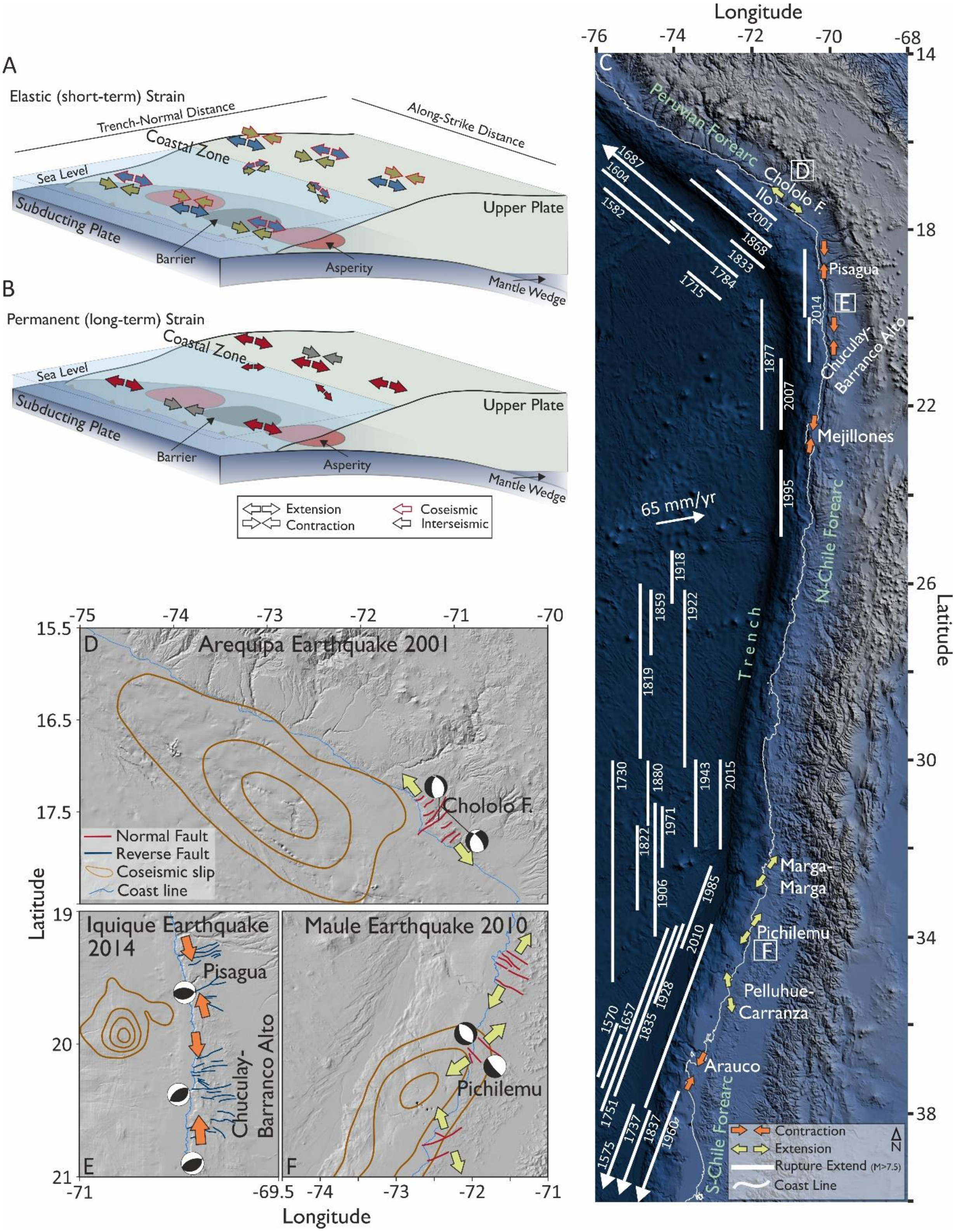

Figure 4: Synthesis of experimental observations and comparison with nature: (A) Trench-parallel strain variations during the seismic cycles and (B) in long-term (100s of seismic cycles). Convergence and divergence arrows represent contraction and extension. Smaller arrows show the oblique strain. In (A), the arrows with red and black outlines indicate coseismic and

interseismic strain states, respectively. (C) Spatial relationships of selected upper-plate faulting events to megathrust earthquakes extend along the South American subduction system (Saillard et al., 2017; Vigny and Klein, 2022 and references therein). (D-F) Location of the upper-plate trench-normal and trench-oblique active faults relative to the slip extends of the recent megathrust events (For references we refer to text).

Supplemental Material.

The supporting material contains additional text, three figures, and a table in a single file supporting the lines of argumentation in the main manuscript (https://doi.org/10.1130/G51115.1).